# ISSN: 2673-5350

## SINGLE-SHOT ELECTRON BUNCH PROFILE MONITOR BASED ON COHERENT TRANSITION RADIATION IMAGING

A. Guisao-Betancur<sup>\*,1</sup>, C. P. Welsch<sup>1</sup>, J. Wolfenden<sup>1</sup>, University of Liverpool, Liverpool, UK O. Grimm, E. Mansten, S. Thorin, MAX IV, Lund University, Lund, Sweden J. Lundquist, Department of Physics, Lund University, Lund, Sweden <sup>1</sup>also at the Cockcroft Institute, Daresbury, UK

Abstract

The development of longitudinal diagnostics for shortpulse electron accelerators is challenging but necessary to provide high-brightness electron bunches. This is equally true in novel plasma accelerators and for free electron lasers. The gold standard for such measurements is the transverse deflecting cavity (TDC); however, these devices are typically invasive and costly to produce and operate. As an alternative, a THz-based reflective imaging system has been designed and installed at the MAX IV short pulse facility (SPF) for imaging coherent transition radiation (CTR) for bunch profile reconstruction. This contribution presents the progress towards applying transfer learning to deep learning models for evaluating the reconstruction of bunch profiles from experimentally acquired CTR images, building on previous successes in profile prediction using simulated data. Practical resolution limits and the next steps in the development of the monitor are also discussed, where the reconstructions of the longitudinal profile will be achieved using single-shot CTR images and benchmarked against the TDC bunch profiles.

#### INTRODUCTION

Ultra-short bunch length measurements are crucial in novel facilities such as high-gradient plasma-based accelerators and light sources like free electron lasers (FELs), where high-quality electron bunches on the femtosecond (fs) range are required. This range poses significant challenges for the development of beam instrumentation and diagnostics [1].

Although transverse deflecting cavities (TDCs) are the gold standard for longitudinal phase space characterization, including bunch profile and length measurements [2-5], minimally or non-invasive setups often rely on radiative techniques instead. In such cases, polarization radiation [6] is produced when the bunch charge is made to emit broadband radiation, which is then studied. Some examples of polarization radiation include Cherenkov (ChR) [7], Smith-Purcell (SPR) [8,9], and transition radiation (TR) [10]. In all cases, radiation will be coherent for all the wavelengths that are equal to or longer than the bunch length itself, and the analysis can be done using either spectral [10, 11] or time domain methods.

For spectral analysis, the spectral distribution is analyzed using iterative phase retrieval algorithms, knowing that the spectrum of the coherent radiation  $S(\rho(z), \omega)$  is given by:

$$S(\rho(z), \omega) = S_n(\omega)[N + N(N-1)F_z(\rho(z), \omega)],$$

where  $S_p(\omega)$  is the single particle spectrum, N the number of particles in the bunch, and  $F_z(\rho(z), \omega)$  the longitudinal form factor [12]. The longitudinal form factor carries information about the bunch profile since it is defined as the modulus squared of the Fourier transform of the longitudinal particle distribution  $\rho(z)$ :

$$F_z(\rho(z),\omega) = \left| \int_{-\infty}^{\infty} \rho(z) e^{-i\frac{\omega}{c}z} dz \right|^2.$$

However, the spatial distribution of the image in coherent transition radiation (CTR) has also been proven to contain information about the bunch profile [13]. The image distribution for an electron bunch  $I_{\text{bunch}}^{i}$  for a specific bandwidth is given by:

$$\frac{dI_{\rm bunch}^i}{dr} \approx N_e^2 \int_{\Delta\omega} \frac{d^2 I_e^i}{d\omega dr} F_z(\rho(z), \omega) d\omega \,,$$

where  $I_e^i$  is the image distribution for a single electron and  $\Delta \omega$  is the bandwidth [13, 14]. With the imaging approach, other sources of radiation, such as synchrotron radiation, become defocused and flattened in the background since they originate outside the TR source plane.

The analysis of the resulting CTR images is not straightforward, as the information about the bunch profile is encoded in the spatial distribution alongside external effects from the optics and detector used, for example. This motivates the use of deep learning to reconstruct the bunch profiles by learning these complex patterns from large amounts of simulated data and transferring the knowledge (transfer learning) to perform reconstructions from the more limited amount of experimental data.

#### SETUP AND CTR IMAGING SYSTEM

The CTR imaging system was designed for installation at the MAX IV short pulse facility (SPF) (see Fig. 1), where it is possible to test with 3 GeV e-beams. SP01 and SP02 are located within the SPF, where the former is the diagnostic beamline containing the high-energy TDC, and the latter is the beamline connecting to FemtoMAX (i.e., to the users) and where the CTR target actuator and imaging system are located.

In the setup (schematic shown in Fig. 2) the production of CTR is achieved by placing with an actuator a 25 mm diameter, 5 mm thick aluminum substrate with a 200 nm gold

<sup>\*</sup> A.M.Guisao-Betancur@liverpool.ac.uk

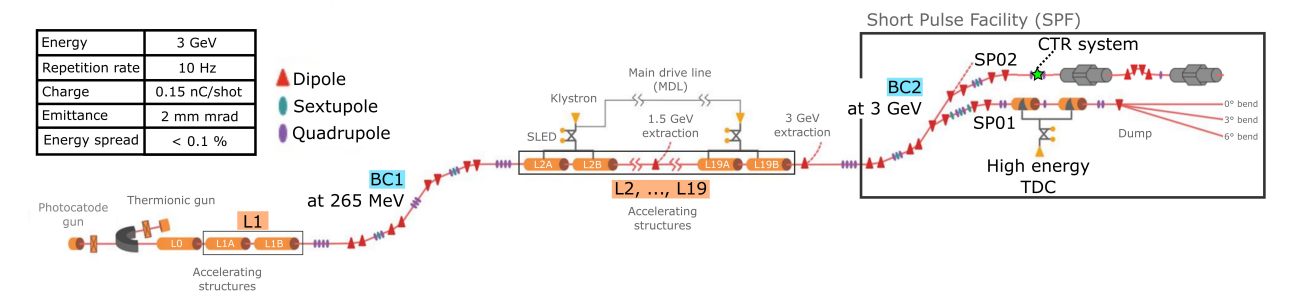


Figure 1: Layout of the MAX IV linac and the SPF. Highlighted are the interest points for the parameter scans at linacs L1 and L2-19 (orange) and the bunch compressors BC1 and BC2 (blue). At the SPF, the SP01 arm contains the high energy TDC, and the SP02 arm is where the CTR imaging system is located. Adapted from LEDS workshop 2024 slides "Characterisation of the MAX IV arc compressors using an S-band deflector".

layer finish surface into the path of the e-beam to intercept it. By setting the target at a 45° incidence, the backward transition radiation can be studied, as it emerges perpendicular to the beamline and can be observed through an HRFZ-Si window. Imaging the coherent transition radiation required the design of a broadband imaging system composed of two 1" off-axis parabolic (OAP) silver-coated mirrors (reflected focal lengths (RFL) 4" and 8", for a 2× magnification) and a 160 × 160 pyroelectric array (Pyrocam™ IIIHR GigE: PY-III-HR-C-A-PRO).

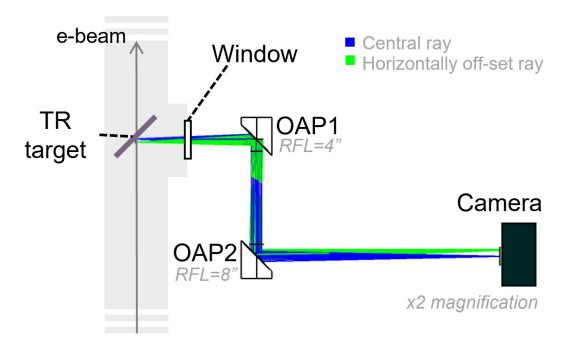


Figure 2: Schematic of the CTR production (TR target at 45° intercepting the e-beam) and the optical system for imaging (viewing window, system of two OAPs in antisymmetric configuration and pyroelectric array).

Simulations using Zemax OpticStudio predicted the presence of geometric aberrations on the horizontal axis of the system caused by the antisymmetric configuration of the OAP mirrors, which were also observed in the experimental data (see Fig. 3). Although this would make the direct analysis of the spatial distribution of the CTR images difficult, it is expected that the deep learning models would learn all the image features, including these aberrations, since they are equally present in the simulated data, thus not affecting the reconstruction after the knowledge transfer.

## DATASETS AND MODEL TRAINING

Simulated and experimental datasets are considered for this reconstruction problem to train the source (first) and tar-

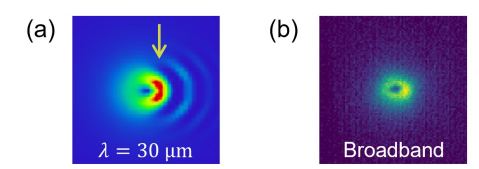


Figure 3: (a) Resulting simulated image for a single wavelength on the antisymmetric configuration of the OAPs, emphasis on the horizontal asymmetry, and (b) single-shot experimental CTR image sample.

get (second) models, respectively. Samples of the simulated and experimental bunch current profiles are shown in Fig. 4.

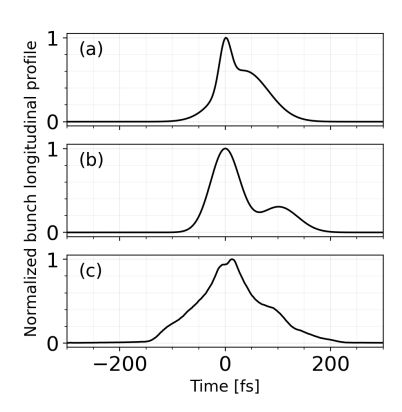


Figure 4: Samples of simulated double Gaussian bunch profiles for (a) dataset 1, (b) dataset 2, and (c) experimental shot from the TDC.

For the training, simulated datasets were generated with 20000 samples of CTR image and current profile pairs using Zemax OpticStudio simulations. Dataset 1 is composed of combinations of two Gaussians with full-width half maximum FWHM ranges of [10, 100] and [100, 300] fs, respectively, where the second Gaussian must be <40 % the amplitude and within one standard deviation  $\sigma$  of the first one. For dataset 2, more variance was introduced to test the generalization ability of the trained model, with FWHM ranges

ISBN: 978-3-95450-262-2 ISSN: 2673-5350 doi: 10.18429/JACoW-IBIC2025-WEPCO01

of [1, 100] and [50, 300] fs, with the second Gaussian up to 100% of the amplitude and within  $3\sigma$  of the first one.

The experimental datasets were taken at the MAX IV SPF, performing 1D and 2D phase (linacs (i) L1 and (ii) L2-19 in Fig. 1) and sextupole (bunch compressors (i) BC1 and (ii) BC2 in Fig. 1) parameter scans. For the same parameter ranges, the bunch profiles are extracted from the TDC images taken in SP01, and the CTR images were taken on SP02, although at different moments during the beamtime. The preprocessing and consolidation of the experimental datasets are still ongoing.

Figure 5 presents the ensemble deep learning model, inspired by the developments in Ref. [15], used for these preliminary results. The input is the CTR image, and the output is the reconstructed bunch profile.

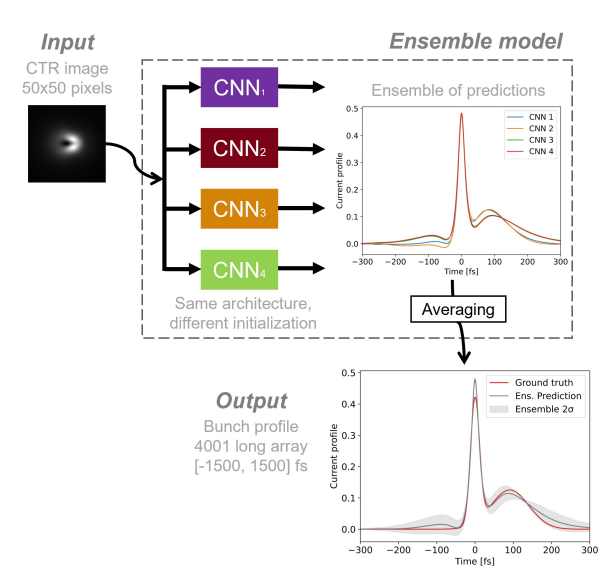


Figure 5: Schematic of the ensemble models for bunch profile reconstruction. The CTR image acts as input. Four convolutional neural networks (CNNs) with the same architecture but trained with different initialization parameters produce four distinct reconstructions, and the output and uncertainty are obtained by averaging.

These preliminary results are for an ensemble model trained with dataset 1 and further tested on dataset 2. The performance on unseen data is shown in Fig. 6. The median value of the training metric, mean squared error (MSE), for 500 unseen samples in dataset 1 is  $5.95 \times 10^{-5}$ , which grows to  $3.44 \times 10^{-4}$  when testing on dataset 2, as can be visualized in Fig. 6 (a). This behavior is expected, as the latter contains completely new data with higher variance. However, it was still possible to reconstruct bunch profiles when the smaller Gaussian was not shorter than 10 fs; below this value, the uncertainty on the predictions (see Fig. 6 (b)) shows that the results are not reliable. This hard limit at 10 fs is expected due to the information loss caused by the low transmittance of the HRFZ-Si window in the required wavelength range.

Adding up the uncertainties for all points in the reconstructed bunch profile yields the cumulative uncertainty pre-

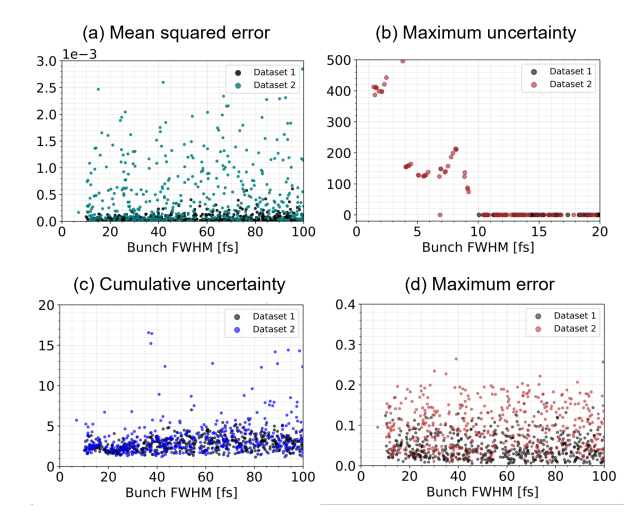


Figure 6: Performance metrics for bunch profile reconstruction from unseen CTR images from dataset 1 and dataset 2, with model trained on dataset 1 without fine-tuning. (a) Mean squared error - MSE (model training metric), (b) maximum uncertainty on reconstructions on the [1, 20] fs range, (c) cumulative uncertainty (added uncertainty of all the full bunch profile points), and (d) maximum error.

sented in Fig. 6 (c), which is mainly kept in a consistent range between the two datasets, with slightly worse performance in dataset 2. Lastly, the maximum error (calculated as the maximum difference error for a given bunch profile) can be nearly double for dataset 2, which accounts for the higher variance in the parameter ranges of the Gaussians in this second dataset.

## CONCLUSIONS

Comparisons have been made between models trained and tested on different datasets with varying ranges of Gaussian parameters. The models have successfully reconstructed unseen bunch profiles with double Gaussian combinations in a range of higher variance. The pre-training phase for the transfer learning has been completed by using these simulated double Gaussian datasets. The extraction of experimental data for future fine-tuning and testing is advanced. Still, additional preprocessing will be necessary before fine-tuning the models to achieve successful knowledge transfer and single-shot experimental reconstruction of bunch profiles in the fs range.

### **ACKNOWLEDGEMENTS**

This project has received funding from the European Union's Horizon Europe research and innovation program under grant agreement no. 101073480 and the UKRI guarantee funds, the Cockcroft Institute core grant no. STFC ST/V001612/1, and the AWAKE-UK phase II project funded by STFC under grant no. ST/X005208/1.

## REFERENCES

- [1] M. C. Downer et al., "Diagnostics for plasma-based electron accelerators", Rev. Mod. Phys., vol. 90, no. 3, p. 035002, 2018. doi:10.1103/RevModPhys.90.035002
- [2] C. Behrens *et al.*, "Few-femtosecond time-resolved measurements of X-ray free-electron lasers", *Nat. Commun.*, vol. 5, pp. 1–7, 2014. doi:10.1038/ncomms4762
- [3] J. Maxson *et al.*, "Direct measurement of sub-10 fs relativistic electron beams with ultralow emittance", *Phys. Rev. Lett.*, vol. 118, no. 15, p. 154802, 2017. doi:10.1103/PhysRevLett.118.154802
- [4] E. Prat *et al.*, "Sub-femtosecond time-resolved measurements of electron bunches with a C-band radio-frequency deflector in x-ray free-electron lasers", *Rev. Sci. Instrum.*, vol. 94, no. 4, p. 043302, 2023. doi:10.1063/5.0144876
- [5] E. Prat et al., "Attosecond time-resolved measurements of electron and photon beams with a variable polarization Xband radiofrequency deflector at an X-ray free-electron laser", Adv. Photon., vol. 7, no. 2, p. 026002, 2025. doi:10.1117/1.AP.7.2.026002
- [6] D. V. Karlovets and A. P. Potylitsyn, "Universal description for different types of polarization radiation", Aug. 2009, arXiv:0908.2336 [physics.acc-ph]. doi:10.48550/arXiv.0908.2336
- [7] A. Curcio *et al.*, "Noninvasive bunch length measurements exploiting Cherenkov diffraction radiation", *Phys. Rev. Accel. Beams*, vol. 23, no. 2, p. 022802, 2020. doi:10.1103/PhysRevAccelBeams.23.022802
- [8] I. V. Konoplev et al., "Single shot, nondestructive monitor for longitudinal subpicosecond bunch profile measurements with femtosecond resolution", Phys. Rev. Accel. Beams, vol. 24, no. 2, p. 022801, 2021. doi:10.1103/PhysRevAccelBeams.24.022801

- [9] H. Yamada *et al.*, "Study of coherent Smith–Purcell radiation in the terahertz region using ultra-short electron bunches", *Particles*, vol. 6, no. 3, pp. 693–702, 2023. doi:10.3390/particles6030042
- [10] O. Zarini *et al.*, "Multioctave high-dynamic range optical spectrometer for single-pulse, longitudinal characterization of ultrashort electron bunches", *Phys. Rev. Accel. Beams*, vol. 25, no. 1, p. 012801, 2022. doi:10.1103/PhysRevAccelBeams.25.012801
- [11] B. Schmidt et al., "Benchmarking coherent radiation spectroscopy as a tool for high-resolution bunch shape reconstruction at free-electron lasers", Phys. Rev. Accel. Beams, vol. 23, no. 6, p. 062801, 2020. doi:10.1103/PhysRevAccelBeams.23.062801
- [12] A. Gillespie, "Bunch length diagnostics: Current status and future directions", in *Proc. 2018 CERN-Accelerator-School Course on Beam Instrumentation*, Tuusula, Finland Jun. 2018, pp. 314–363.
- [13] J. Wolfenden *et al.*, "Coherent transition radiation spatial imaging as a bunch length monitor", in *Proc. IPAC'19*, Melbourne, Australia, May 2019, pp. 2713–2716. doi:10.18429/JACoW-IPAC2019-WEPGW095
- [14] A. G. Shkvarunets and R. B. Fiorito, "Vector electromagnetic theory of transition and diffraction radiation with application to the measurement of longitudinal bunch size", *Phys. Rev. Spec. Top. Accel. Beams*, vol. 11, no. 1, p. 012801, 2008. doi:10.1103/PhysRevSTAB.11.012801
- [15] O. Convery *et al.*, "Uncertainty quantification for virtual diagnostic of particle accelerators", *Phys. Rev. Accel. Beams*, vol. 24, no. 7, p. 074602, 2021. doi:10.1103/PhysRevAccelBeams.24.074602